HHS Public Access

Author manuscript

Nat Mater. Author manuscript; available in PMC 2018 October 01.

Published in final edited form as:

Nat Mater. 2017 October ; 16(10): 1029–1037. doi:10.1038/nmat4972.

Long-lived force patterns and deformation waves at repulsive epithelial boundaries

Pilar Rodríguez-Franco[1], **Agustí Brugués**[1], **Ariadna Marín-Llauradó**, **Vito Conte**[1], **Guiomar Solanas**[3], **Eduard Batlle**[3,4], **Jeffrey J Fredberg**[5], **Pere Roca-Cusachs**[1,6], **Raimon Sunyer**[1,2,*], and **Xavier Trepat**[1,2,4,6,*]

[1]Institute for Bioengineering of Catalonia, Barcelona 08028, Spain

[2]Centro de Investigación Biomédica en Red en Bioingeniería, Biomateriales y Nanomedicina, 28029 Madrid, Spain

[3]Institute for Research in Biomedicine (IRB Barcelona), The Barcelona Institute of Science and Technology, 08028 Barcelona, Spain

[4]Institució Catalana de Recerca i Estudis Avançats (ICREA), Barcelona, Spain

[5]Harvard T. H. Chan School of Public Health, Boston, Massachusetts

[6]University of Barcelona, 08028 Barcelona, Spain

Abstract

For an organism to develop and maintain homeostasis, cell types with distinct functions must often be separated by physical boundaries. The formation and maintenance of such boundaries are commonly attributed to local mechanisms restricted to the cells lining the boundary. Here we show that, besides these local subcellular mechanisms, the formation and maintenance of tissue boundaries involves long-lived, long-ranged mechanical events. We analyzed the formation of repulsive epithelial boundaries between two epithelial monolayers, one expressing the receptor tyrosine kinase EphB2 and one expressing its ligand ephrinB1. Upon contact, both monolayers exhibited oscillatory patterns of traction forces and intercellular stresses that spanned several cell rows and tended to pull cell-matrix adhesions away from the boundary. With time, monolayers jammed and supracellular force patterns became long-lived, thereby permanently sustaining tissue segregation. Jamming was paralleled by the emergence of deformation waves that propagated away from the boundary. This phenomenon was not specific to EphB2/ephrinB1 repulsion but was also present during the formation of boundaries with an inert interface and during fusion of homotypic epithelial layers. Our findings thus unveil a global physical mechanism that sustains tissue separation independently of the biochemical and mechanical features of the local tissue boundary.

[*]Correspondence to: rsunyer@ibecbarcelona.eu, xtrepat@ibecbarcelona.eu.

Author contributions

P.R-F., A.B. and X.T. designed experiments. P.R-F., A.B., A.M-L, and R.S. performed experiments. P.R-F. and R.S. designed magnetic stencils and contributed to protocol design. P.R-F., A.B., R.S., A.M-L and V.C. carried out data analysis. G.S. and E.B. provided cell lines, characterized cell lines, and contributed to protocol design. E.B, J.J.F and P.R-C contributed to data interpretation. All authors discussed and interpreted results. P.R-F and X.T. wrote the manuscript with feedback from all authors. X.T. oversaw the project.

The animal body is organized in functional compartments separated by physical boundaries. In development, embryonic boundaries ensure functional tissue segregation during large scale movements such as gastrulation, and during highly proliferative events such as growth of imaginal discs[1]. Besides this segregation role, embryonic boundaries are also important signaling centers that determine tissue patterning[2]. Most embryonic boundaries are eventually filled with extracellular matrix (ECM), which provides a permanent physical barrier between tissues during adult life. However, some adult epithelial tissues maintain compartmentalization and architecture through functional barriers devoid of ECM[1]. These barriers have been shown to constrain tumor growth, and their disruption is associated with increased malignancy in a diversity of cancers such as colorectal, breast, and prostate cancer[3,4].

While the importance of tissue boundaries has been recognized for centuries[5]our modern understanding of underlying mechanisms began in the 1950s with the differential adhesion hypothesis, which states that tissues segregate by differences in effective surface tension[6]. Such differences were initially attributed to variations in the type or expression level of cellcell adhesion proteins[7]. Later on, this picture was completed with the notion that differences in contractile cortical tension must also be taken into account to explain tissue segregation[8–11].

An alternative mechanism for tissue segregation is based on repulsive cell-cell interactions rather than differential adhesion[1]. A paradigmatic example of a cellular repulsion mechanism is bi-directional signaling between the Eph tyrosine kinase receptors and their ligands ephrins. When Eph and ephrin are selectively expressed in two adjacent cell populations, their interaction prevents the formation of cadherin-based adhesions, thus promoting tissue segregation. Cell repulsion mediated by Eph/ephrin interactions has been reported in non-epithelial cells such as neurons and somites, but also in epithelial tissues such as the intestinal epithelium[12]. In these tissues, EphB receptors are expressed by cells localized at base of the crypts whereas ephrinB ligands shows a complementary domain within the differentiation compartment. Mice mutant for EphB2, EphB3 or ephrinB1 display defects in tissue compartmentalization, which include mispositioning of Paneth cells and aberrant nondirectional migration of epithelial progenitor cells[13,14]. Mechanisms that have been proposed to account for cell repulsion during Eph/ephrin interactions include proteolytic cleavage of the extracellular domain of ephrin[15,16] or E-cadherin[17], endocytosis of Eph/ephrin complexes[18,19], and retraction of adhesive contacts mediated by actomyosin contractility[20–22].

In addition to adhesive and repulsive interactions at the molecular scale, dynamics of tissue segregation also involves multiscale cellular movements, deformations, rearrangements and forces[1,9–11,23–26]. How these mechanical quantities and their mutual relationships are related to the local interaction at the segregation boundary is largely unknown. Here we examined epithelial mechanics during the formation and maintenance of distinct types of simple unidimensional boundaries. We show that, irrespective of the nature of the local repulsive interaction, boundary formation involves long-lived and long-ranged mechanical force patterns, and propagation of deformation waves. These phenomena are intrinsically

associated with monolayer jamming and they are unanticipated by current theories of tissue segregation.

We fabricated magnetic PDMS stencils comprising two large compartments separated by a thin barrier, and attached them on top of collagen-coated soft polyacrylamide gels. In one compartment of the stencil we seeded MDCK cells expressing the EphB2 receptor and in the other cells expressing its ligand ephrinB1 (Fig. 1a, see Supplementary Fig. 1 for a characterization of expression levels and localization of EphB2 and ephrinB1). After allowing cells to adhere and form a cohesive monolayer, the PDMS stencil was removed and monolayers migrated towards each other as extensively described in classical scratch-wound assays (Fig 1b,c)[27,28]. Unlike in these assays, however, when the two cell populations collided they formed a wavy boundary that progressively straightened out with time (Fig. 1c) (Supplementary Video 1, Supplementary Fig. 2). Immunostainings revealed an empty micron-sized band between the two cell populations with the eventual presence of short-lived lamellipodia and filopodia that transiently extended under the opposite edge. Straightening out of the boundary was paralleled by the formation of a supracellular actomyosin cable at the edge of each monolayer (Fig. 1d-k). E-cadherin was present at the junctions between cells comprising each population, but was absent from the boundary (Fig. 1l-o). This behavior is unlike the collision between two populations of the same type, which fuse shortly after contact, rapidly creating a single cohesive cell monolayer[27] (Supplementary Video 1).

Following the removal of the PDMS stencil, cells located at both monolayer edges increased their area and oriented their body and nuclei in the direction of cell motion (Fig. 1p). Shortly after collision (Fig. 1p, arrows), these cells reversed their orientation and aligned parallel to the boundary. Eventually, oriented cell division restored an isotropic distribution of cell shape (Supplementary Fig. 3). The process of boundary formation was paralleled by a pronounced increase in cell density throughout the monolayers due to proliferation and migration of cells into the boundary area (Fig. 1p). The first phase of the experiments, in which monolayers approach each other and cell density decreases, will be hereafter referred to as the unjamming phase (Fig. 1c). Conversely, the second phase, in which the boundary forms and cell density increases, will be referred to as the jamming phase.

To study mechanics of boundary formation, we used traction force microscopy to measure forces at the cell-substrate interface. Throughout the experiments, traction maps exhibited large dynamic fluctuations both at the monolayer edges and behind them (Fig. 2a-h, Supplementary Video 2). To distinguish fluctuations from systematic traction patterns, we averaged the component normal to the boundary ($T_{\perp}$) over the y coordinate, thereby reducing the dimensionality of the system to only one spatial dimension and one temporal dimension (see methods). Data were then represented as kymographs[25,29] (Fig. 2m, see Supplementary Fig. 4 for experimental repeats of kymographs). During the unjamming phase, kymographs of $T_{\perp}$ displayed well-known features of monolayer expansion such as a decay of average tractions away from the leading edges[30,31]. By contrast, during the jamming phase kymographs revealed long-lived spatial oscillations of traction forces (Fig 2m,q). These spatial oscillations did not attenuate in space or propagate in time. The autocorrelation function $C_{TT\perp}$ of the traction kymographs during the jamming phase

revealed a characteristic spatial period of 52±9 μm, corresponding to ~4 cell diameters (Fig. 2s). Traction oscillations were predominantly negative in the EphB2 monolayer, and predominantly positive in the ephrinB1 monolayer. Thus, several rows of cells were found to pull on cell-substrate adhesions away from the boundary, and did so using remarkable oscillatory patterns.

To assess how these mechanical patterns affected tension within and between cells we computed the 2D stress tensor in the monolayer using monolayer stress microscopy (MSM)[32]. The 2D average normal stress ($\bar{\sigma}$) showed dynamic heterogeneities and, as jamming progressed, it increased with distance from the boundary (Fig. 2i-l, Supplementary Video 3). This was confirmed in kymographs of the projection of the stress tensor along the direction normal to the boundary ($\sigma_{\perp}$), which showed markedly distinct spatial patterns during the unjamming and jamming phases (Fig. 2n, Supplementary Fig. 4b). During the unjamming phase, $\sigma_{\perp}$ built up quickly within the first few cell rows and reached a plateau thereafter. Upon contact, $\sigma_{\perp}$ decayed sharply and then exhibited progressive buildup that was stabilized in time as monolayers jammed (Fig. 2n). Throughout the process of boundary formation, $\sigma_{\perp}$ was positive at the boundary and behind it thus indicating that cells are under tension. The term “repulsive interaction”, as is often used to describe the Eph/ephrin interaction, is thus not strictly correct from a mechanical perspective because repulsive interactions are based on compression rather than tension. Together, our force measurements establish that the formation of EphB2/ephrinB1 barriers involves not only local events at the boundary, but also the mechanical cooperation of many cells located behind it. This cooperation leads to supracellular mechanical patterning that pulls cell-substrate adhesions away from the boundary.

We next investigated the mechanism by which traction and intercellular stress patterns become long-lived. We hypothesized that this mechanism could involve cell jamming induced by increased cell density[24–26,33–35]. To test this hypothesis, we carried out boundary formation experiments using cells in which proliferation had been inhibited with thymidine (Supplementary Fig. 5f). Like control experiments, non-proliferative monolayers approached each other and formed a stable boundary. Traction kymographs showed oscillatory patterns with a spatial period similar to that of controls (51±7 μm, Fig. 2o,t). However, compared to control experiments, traction oscillations did not show an offset of opposite sign at each side of the boundary (Fig. 2q). As a consequence, the increase in $\sigma_{\perp}$ with distance was smaller than in controls (Fig. 1p,r). These experiments suggest that cell jamming stabilizes EphB2/ephrinB1 boundaries by enhancing the buildup of intercellular forces behind the boundary.

To further understand the role of jamming during boundary formation, we measured cell velocities (V) using particle imaging velocimetry (PIV) (Supplementary Video 4). Maps of the horizontal velocity component V_x revealed a phase of fast cohesive motion during unjamming, followed by a progressive slowing down of monolayer kinematics during jamming (Fig. 3a-h). Strikingly, the monolayer did not show a full kinetic arrest as previously reported in monolayers of growing density[33]. Instead, pulses of velocity emerged in cooperative cell packs close to the monolayer boundary and propagated backwards across the monolayers. These packs can be clearly appreciated upon thresholding velocity maps to separate rapid propagating cells from slow non-propagating cells (Fig. 3i-k, Supplementary

Video 4). Sudden calcium chelation abrogated the wave fronts, indicating that waves propagate through cell-cell junctions (Supplementary Fig. 4, Supplementary Video 5).

To further characterize these waves we computed kymographs of the normal component to the boundary ($V_\perp$) (Fig. 3l). These kymographs showed an unremarkable initial phase of cohesive approach of the two monolayers. After monolayer collision, however, kymographs displayed pronounced diagonal bands in the ephrinB1 monolayers, which reveal wave fronts that are launched at the boundary and propagate until reaching the limits of the field of view without significant attenuation. Because of the continuous nature of monolayers, front propagation in the velocity field is indicative of a deformation wave. This was confirmed by kymographs of the strain rate $\dot{\varepsilon}_\perp$, which showed propagating fronts of cell compression and extension (Fig. 3m). To study the spatial extent of front propagation we carried out experiments tiling several fields of views (Supplementary Fig. 7, Supplementary Video 6). These experiments revealed a characteristic propagation distance longer than 1 mm before attenuation.

To better characterize deformation waves we computed the autocorrelation function $C_{VV\perp}$ of the monolayer velocity kymographs $V_\perp$ during the jamming phase (Fig. 3n). $C_{VV\perp}$ displayed a diagonal band originating at τ=0min and R=0μm and spanning an interval longer than 100 min and 200 μm in time and distance, respectively. This diagonal band demonstrates the propagation of a deformation wave with a speed corresponding to the inverse of the slope (117 μm/h). Besides this dominant band in the correlation function, several parallel secondary bands of similar slope were observed, indicating multiple propagation events of similar velocity.

To test whether jamming was required for wave propagation we analyzed velocity maps and kymographs of non-proliferative cell monolayers (Fig. 4a-h, Supplementary Video 7). Kymographs of $V_\perp$ showed that propagating fronts were less abundant and less pronounced than in controls (Fig. 4q), as indicated by a broader diagonal band in $C_{VV\perp}$ (Fig. 4r). Jamming thus appears to favor wave propagation. To further study the mechanism underlying propagation we inhibited myosin activity using blebbistatin (Fig. 4i-p). This treatment largely inhibited traction forces and the formation of actomyosin cables at the boundary, but it did not prevent tissue segregation (Supplementary Fig. 8, Supplementary Video 8). Deformation waves were largely absent from kymographs, indicating that their propagation requires monolayer tension (Fig. 4s,t).

We next asked whether deformation waves are specific to the EphB2/ephrinB1 interaction, or whether they are instead a more general feature of repulsive epithelial interfaces. To this end, we replaced the ephrinB1 monolayer with a PDMS wall and analyzed dynamics after the collision between the EphB2 monolayer and the wall (Fig 5a-i). Like the case of the EphB2/ephrinB1 boundary, several wave fronts emerged at the EphB2/PDMS boundary and propagated for tens of cell diameters (Fig. 5j,k). These experiments establish that mechanical waves are not triggered by a specific chemical interaction at the boundary. Rather, they appear to be a generic feature of repulsive epithelial interfaces during jamming.

This sticking observation led us to ask whether waves also emerge during the collision between two identical monolayers. Upon contact, such monolayers fuse through attractive cadherin interactions but they repel each other through volume exclusion, thus raising the possibility that deformation waves are also launched at the homotypic interface. To test this possibility, we studied homotypic collisions between EphB2/EphB2 and ephrinB1/ephrinB1 monolayer pairs (Fig. 6, Supplementary Videos 9,10). Similar to the case of EphB2/ephrinB1 experiments, contact between homotypic monolayers caused boundary cells to align parallel to the edge (Supplementary Fig. 9). However, these cells relaxed towards an isotropic shape significantly faster than cells at EphB2/ephrinB1 contact. Shortly after contact, no visual sign of a boundary remained (Supplementary Videos 1,9,10). Both EphB2 and ephrinB1 monolayers exhibited waves that were launched close to the contact point and propagated away from it at 85±17 μm/h (EphB2/EphB2) and 112±20 μm/h (ephrinB1/ephrinB1). This finding indicates that the fused epithelium retains mechanical memory of the contact line well after fusion. It shows, further, that propagation of mechanical waves is a general property of epithelial contacts as long as they are jammed.

Our study unveils two unanticipated mechanical features of epithelial monolayers at repulsive interfaces. Firstly, we identified long-lived oscillatory traction patterns with a characteristic length scale of several cell diameters. These patterns tend to pull cell-substrate adhesions away from the interfaces and give rise to a gradient of intercellular stress. It is worth noting that the boundary formed even when contractility was inhibited with blebbistatin (Fig. 4). Thus, while the local actomyosin cable and the supracellular contractile structures tend to sustain epithelial segregation, additional mechanisms independent of contractility must be invoked to explain boundary formation by EphB2/ephrinB1 interactions.

Secondly, we showed that deformation waves are triggered at the epithelial interface and propagate across the monolayer. Waves observed here are not specific to a chemical interaction at the boundary but rather appear to be a generic feature of jammed epithelial contacts. Propagation of mechanical waves has been observed in a diversity of inert and living jammed systems, ranging from driven suspensions of hard sphere colloids to epithelial monolayers[36–42]. Wave propagation in underdamped inertial systems ordinarily stems from an exchange between elastic potential energy and kinetic energy. Within the epithelial monolayer, however, inertial effects are vanishingly small, and for that reason the layer would be expected to be highly overdamped. Accordingly, the existence of underdamped wave-like phenomena has led to the suggestion that other factors can interact dynamically so as to introduce another time scale into the system and thereby create an ‘effective inertia’[43,44]. Such an effective inertia would allow the system to sustain the propagation of underdamped waves. For example, the class of models advanced by Vicsek and colleagues assumes that the direction of the local particle velocity vector reflects a competition between the velocities of neighboring particles and random noise[45,46]. At intermediate noise levels, such models predict a coupling of density to order in a manner that causes emergence of traveling density waves[47–49]. More recently it has been shown that there exists a feedback within the epithelial layer between mechanical strain and cellular contraction which, together with cellular elasticity, can sustain oscillations and waves[44]. Still other possibilities are time scales introduced by cycles of strain-induced cytoskeletal reinforcement versus

fluidization[50,51], strain-induced polarization versus contractility[43,44], and strain-dependent dynamics involving Rac1, the tumor suppressor merlin, and cell polarization[40,42]. The extent to which current models predict travelling waves at jammed epithelial boundaries is yet to be assessed. More generally, further research should identify feedback mechanisms and molecular players that underlie to emergence of ‘effective inertia’ in monolayers.

Traction patterns and deformation waves at repulsive and attractive interfaces are emergent features associated with the proximity of the monolayer to a jammed state. Thus, beyond providing a mechanism for kinetic arrest, as seen in inert matter[52,53], cell jamming gives rise to non-trivial biological patterns and propagation phenomena in active matter. Importantly, repulsive cell interfaces during development are often paralleled by waves and oscillations that give rise to tissue patterning[2,54,55]. Current understanding emphasizes that these waves and oscillations act upstream of boundary formation and are controlled by genetic clocks[56]. Here we identified that a physical boundary is sufficient to trigger differentials of cellular forces and deformations, and that jamming is sufficient to control the dynamics of those differentials. Our findings thus raise the possibility that rather than being solely controlled by genetic clocks and travelling waves of biochemical nature, tissue segregation and patterning during development and homeostasis is controlled by cell jamming[57].

Materials and Methods

Cell generation and sorting

Generation of MDCK cells expressing either EphB2 or ephrinB1 ligands was described elsewhere[59]. Briefly, MDCK cells were infected with lentivirus carrying EphB2 or ephrinB1 complementary DNAs. The canine E-cadherin–GFP fusion construct (gift from J.W. Nelson) was inserted downstream of the cytomegalovirus promoter into the FUW lentiviral vector backbone. The E-cadherin–Cherry fusion construct was derived from the E-cadherin–GFP FUW plasmid. Lentiviral particles containing those cDNAS were produced to infect the EphB2-positive (E-cadherin–GFP) or ephrinB1-positive (E-cadherin–Cherry) populations.

MDCK cells expressing homogeneous levels of anti-EphB2-mcherry (ab)/GFP (protein) or anti-ephrinB-GFP (ab)/Cherry (protein) were selected using an ARIA fluorescence-activated cell sorter (BD).

Lifeact Lentiviral transfection

MDCK EphB2/Ephrin expressing cells were infected with lentivirus carrying lifeact-mcherry or lifeact-CFP (gift from J. de Rooij) and FAC sorted using an ARIA fluorescence-activated cell sorter (BD).

Cell culture

MDCK cells were cultured in minimum essential media (MEM) with Earle’s Salts and l-glutamine (31095-029, Thermofisher) supplemented with 10% fetal bovine serum (FBS; 10270-106, Thermofisher), 100 units ml^{-1} penicillin, 100 μg ml^{-1} streptomycin and 292 μg ml^{-1} l-glutamine (10378-016, Thermofisher). Cells were maintained at 37°C in a humidified atmosphere with 5% CO_2.

Magnetic PDMS stencil preparation

We prepared the magnetic PDMS by mixing thoroughly the base and cross-linker in a 10:1 proportion. Then added 50% (w/w) of magnetite (Inoxia) and mixed for 5 min. Air was removed by placing the mixture in a vacuum jar for 1 h. Afterwards, we filled the master with magnetic PDMS and cured it for 2 h at 60°C.

Design and 3D printing of masters

We used the open source software openSCAD to design the masters for the PDMS stencil replication and also to design a magnet holder to adhere the stencils to the gels. Sketches were exported to a Stereolithography file format file (STL), which is a standard file for 3D printing. An FDM 3D printer was used to print the prototype pieces using the open source software Slic3r (http://slic3r.org/) to obtain the gcode. The final masters were ordered through the 3D printing service of Shapeways (www.shapeways.com).

Polyacrylamide gel preparation

Polyacrylamide gel preparation was adapted from protocols described previously (Kandow, 2007). Glass-bottom dishes were activated by using a 1:1:14 solution of acetic acid/bind-silane/ethanol. The dishes were washed twice with ethanol and air-dried for 10 min. For 15 kPa gels, a 500 µl stock solution containing 93.75 µl acrylamide, 45 µl bisacrylamide, 2.5 µl APS, 0.25 µl TEMED and 3.2 µl of 200-nm-diameter far red fluorescent carboxylate-modified beads was prepared. A drop of 15 µl was added to the centre of the glass-bottom dishes, and the solution was covered with 18-mm-diameter GelBond film coverslips custom cut by an electronic cutting tool (Silhouette Cameo). After polymerization, gels were functionalized with sulfo-sanpah and exposed to UV light for 5 minutes. Then, gels were washed with miliQ water for 5 minutes. Afterwards, gels were washed with PBS and incubated with 100 µl of a collagen I solution (0.1 mg ml^{-1}) overnight at 4°C. Finally, gels were washed once with HEPES and twice with PBS and incubated with cell culture media for 1h.

Eph/ephrin boundary experiments

We autoclaved the magnetic PDMS stencils at 135°C with a dry program. We passivated the stencils by incubating them for 1h in a solution of 2% Pluronic in PBS. Afterwards, we washed the stencils twice in PBS and dried them with a N_2 flux gun. We then washed the polyacrylamide gels twice using PBS and aspirated the PBS. We dried the polyacrylamide gel surface with a N_2 flux. We placed the 6-well dish on a custom made holder containing a neodymium magnet underneath each coverslip position. Afterwards, we placed the magnetic PDMS stencil on top of each gel, making sure there was a flat, homogenous contact between the PDMS and the gel. Finally, we added 150,000 EphB2-cells concentrated in 120 µl of media in the left hollow region defined by the PDMS membrane and 150,000 ephrinB1 cells in the right hollow region. We waited 1 h for cell attachment. We washed the two hollow regions and added media. We then cultured the cells for 4 hours prior to detaching the PDMS stencil from the gel.

Physical barrier experiments

For the physical barrier experiments the surface of a glass bottom petri dish and the contact surface of the PDMS barrier were activated with corona. Immediately after, the PDMS barrier was put in contact with the glass and pressed for a few seconds ensuring that the two surfaces were making contact and the PDMS was properly attached. The barrier was passivated adding 2 ml of 2% pluronic for 1h. Prior to seeding, the petri dish was placed on top of a magnet and blow-dried with nitrogen. Then a single gasket made of magnetic PDMS was inserted to fit in with the barrier. 150,000 cells were seeded and allowed to attach for 5 hours before detaching the gasket from the glass bottom.

Immunofluorescence staining

Immunofluorescence microscopy experiments were carried out by fixing the cells with 3% paraformaldehyde (Sigma-Aldrich) in PBS, permeabilizing with 0.5% Triton X-100 (Sigma-Aldrich) in PBS, and blocking with 10% FBS (Sigma-Aldrich) in PBS. Primary antibodies mouse anti-E-cadherin (610181, BD Biosciences) and rabbit anti-phMLCII (1673674S, Cell Signaling) diluted at 1:400 and 1:200, respectively, in 10% FBS in PBS were incubated for 3 h at room temperature, and were detected using secondary antibodies goat anti-mouse (A11029, Thermofisher) and donkey anti-rabbit (A21245, Thermofisher) diluted at 1:200 in 10% FBS in PBS. Hoechst 33342 (H3570, Thermofisher) and Phalloidin (A22287, Thermofisher) diluted at 1:5000 and 1:40 respectively in 10% FBS in PBS were incubated during 1 h with the secondary antibodies.

Time lapse imaging

Multidimensional acquisition routines were performed on an automated inverted microscope (Nikon Eclipse Ti) equipped with thermal, CO_2 and humidity control, using MetaMorph (Universal Imaging) software. Time-lapse recording started approximately 30 min after removing the PDMS gasket. The interval between image acquisition was 7 min and a typical experiment lasted for 15–20 h. Images were acquired at ×20 for every time point.

Spinning-Disk imaging

A spinning disk microscope (Andor WD) was used for high-resolution image acquisition.

Traction microscopy

Traction forces were computed using Fourier transform based traction microscopy with a finite gel thickness. Gel displacements between any experimental time point and a reference image obtained after monolayer trypsinization were computed using home-made particle imaging velocimetry software[26].

Monolayer Stress microscopy

Monolayer stresses were computed using monolayer stress microscopy[32]. Monolayer stress microscopy uses traction forces and force balance demanded by Newton's laws to map the two-dimensional stress tensor σ in the monolayer. By rotating these stress components at each point in the cell sheet, we computed the magnitude of the two principal stress components σ_{max} and σ_{min} and their corresponding, mutually perpendicular, principal

orientations. For each point in the monolayer, we then computed the average normal stress within and between cells defined as $\bar{\sigma} = (\sigma_{max} + \sigma_{min})/2$. Boundary conditions during the unjamming phase were those described in Serra-Picamal et al[25]. After collision, stress in the boundary region between the two monolayers was set to zero.

Velocity measurements

Velocity fields were computed using custom-made particle image velocimetry software (PIV) on the phase-contrast images. The interrogation window was 96×96 pixels, and the time interval between consecutive analyzed images was 7 min.

Kymography

Monolayer boundaries were drawn by hand using a home-made algorithm which overlaid traction maps on phase-contrast images to improve accuracy. For each pixel of each side of the boundary, we computed the shortest distance to the leading edge. Next we computed the median values of velocities, tractions, monolayer stresses and strain rates of all pixels located at a given distance from the boundary. To that aim, we performed a coordinate system change from Cartesian coordinates to parallel and perpendicular coordinates (with respect to the boundary). Median values of either perpendicular or parallel components were then represented on a unidimensional segment whose width was the mean width of the monolayers. This operation was repeated for each experimental time point.

Autocorrelation calculation

Autocorrelation C_{AA} of the *x-t* kymograph of a variable A was calculated over the area of the kymograph after the epithelial contact using Matlab function *xcorr2,* which computes:

$$C_{AA}(k,l) = \sum_{m=0}^{M-1} \sum_{n=0}^{N-1} A(m,n) \cdot A(m-k, n-l)$$

C_{AA} was normalized to span the range (-1,1).

Single cell Image Segmentation

Single cell segmentation of boundary cells was performed with a semi-automatic method. Cells at the boundary were contoured using Fiji. Custom made software in Matlab was developed to recognize the contours and post-process the geometrical information therein.

Supplementary Material

Refer to Web version on PubMed Central for supplementary material.

Acknowledgments

We thank Carlos Pérez-González for help with viral transfections; Jaume Comas from the Cytometry service of Barcelona Science Park; Carlos Pérez-González, Elsa Bazellieres, Anna Labernadie, Romaric Vincent, and Léo Valon for stimulating discussions; Carme Cortina for the generation of cell lines, and Natalia Castro for technical assistance. This work was supported by the Spanish Ministry of Economy and Competitiveness (AP2010-2026 FPU grant to PR-F, BFU2015-65074-P to XT, BFU2011-23111 to PR-C, RYC-2014-15559 to VC), the Generalitat de Catalunya (2014-SGR-927), and the European Research Council (CoG-616480 to XT), Obra Social “La Caixa”, a

Career Integration Grant within the seventh European Community Framework Programme (PCIG10-GA-2011-303848 to PR-C), and Fundació la Marató de TV3 (project 20133330 to PR-C).

References

1. Fagotto F. Current Topics in Developmental Biology. 2015; 112:19–64. [PubMed: 25733137]
2. Dahmann C, Oates AC, Brand M. Boundary formation and maintenance in tissue development. Nat. Rev. Genet. 2011; 12:43–55. [PubMed: 21164524]
3. Batlle E, et al. EphB receptor activity suppresses colorectal cancer progression. Nature. 2005; 435:1126–1130. [PubMed: 15973414]
4. Noren NK, Foos G, Hauser CA, Pasquale EB. The EphB4 receptor suppresses breast cancer cell tumorigenicity through an Abl–Crk pathway. Nat. Cell Biol. 2006; 8:815–825. [PubMed: 16862147]
5. Lenhoff, SG., Lenhoff, HM., Trembley, A. Hydra and the birth of experimental biology, 1744: Abraham Trembley's Mémoires concerning the Natural History of a Type of Freshwater Polyp with Arms Shaped Like Horns. Boxwood Press; 1744.
6. Steinberg MS. Reconstruction of tissues by dissociated cells. Some morphogenetic tissue movements and the sorting out of embryonic cells may have a common explanation. Science. 1963; 141:401–8. [PubMed: 13983728]
7. Foty RA, Steinberg MS. The differential adhesion hypothesis: a direct evaluation. Dev. Biol. 2005; 278:255–263. [PubMed: 15649477]
8. Harris AK. Is cell sorting caused by differences in the work of intercellular adhesion? A critique of the steinberg hypothesis. J. Theor. Biol. 1976; 61:267–285. [PubMed: 985668]
9. Brodland GW. The Differential Interfacial Tension Hypothesis (DITH): A Comprehensive Theory for the Self-Rearrangement of Embryonic Cells and Tissues. J. Biomech. Eng. 2002; 124:188. [PubMed: 12002128]
10. Maître J-L, et al. Adhesion functions in cell sorting by mechanically coupling the cortices of adhering cells. Science. 2012; 338:253–6. [PubMed: 22923438]
11. Amack JD, et al. Knowing the boundaries: extending the differential adhesion hypothesis in embryonic cell sorting. Science. 2012; 338:212–5. [PubMed: 23066072]
12. Batlle E, Wilkinson DG. Molecular mechanisms of cell segregation and boundary formation in development and tumorigenesis. Cold Spring Harb. Perspect. Biol. 2012; 4:a008227. [PubMed: 22214769]
13. Batlle E, et al. β-Catenin and TCF Mediate Cell Positioning in the Intestinal Epithelium by Controlling the Expression of EphB/EphrinB. Cell. 2002; 111:251–263. [PubMed: 12408869]
14. Cortina C, et al. EphB–ephrin-B interactions suppress colorectal cancer progression by compartmentalizing tumor cells. Nat. Genet. 2007; 39:1376–1383. [PubMed: 17906625]
15. Janes PW, et al. Adam Meets Eph: An ADAM Substrate Recognition Module Acts as a Molecular Switch for Ephrin Cleavage In trans. Cell. 2005; 123:291–304. [PubMed: 16239146]
16. Hattori M, et al. Regulated cleavage of a contact-mediated axon repellent. Science. 2000; 289:1360–5. [PubMed: 10958785]
17. Solanas G, Cortina C, Sevillano M, Batlle E. Cleavage of E-cadherin by ADAM10 mediates epithelial cell sorting downstream of EphB signalling. Nat. Cell Biol. 2011; 13:1100–7. [PubMed: 21804545]
18. Zimmer M, Palmer A, Köhler J, Klein R. EphB–ephrinB bi-directional endocytosis terminates adhesion allowing contact mediated repulsion. Nat. Cell Biol. 2003; 5:869–878. [PubMed: 12973358]
19. Marston DJ, Dickinson S, Nobes CD. Rac-dependent trans-endocytosis of ephrinBs regulates Eph–ephrin contact repulsion. Nat. Cell Biol. 2003; 5:879–888. [PubMed: 12973357]
20. Shamah SM, et al. EphA Receptors Regulate Growth Cone Dynamics through the Novel Guanine Nucleotide Exchange Factor Ephexin. Cell. 2001; 105:233–244. [PubMed: 11336673]
21. Fagotto F, Rohani N, Touret A-S, Li R. A Molecular Base for Cell Sorting at Embryonic Boundaries: Contact Inhibition of Cadherin Adhesion by Ephrin/Eph-Dependent Contractility. Dev. Cell. 2013; 27:72–87. [PubMed: 24094740]

22. O'Neill AK, et al. Unidirectional Eph/ephrin signaling creates a cortical actomyosin differential to drive cell segregation. J. Cell Biol. 2016; 215
23. Foty RA, et al. Surface tensions of embryonic tissues predict their mutual envelopment behavior. Development. 1996; 122:1611–20. [PubMed: 8625847]
24. Nnetu KD, et al. The impact of jamming on boundaries of collectively moving weak-interacting cells. New J. Phys. 2012; 14:115012.
25. Pawlizak S, et al. Testing the differential adhesion hypothesis across the epithelial–mesenchymal transition. New J. Phys. 2015; 17:83049.
26. Tambe DT, et al. And I hope you like jamming too. New J. Phys. 2015; 17:91001.
27. Liang C-C, Park AY, Guan J-L. In vitro scratch assay: a convenient and inexpensive method for analysis of cell migration in vitro. Nat. Protoc. 2007; 2:329–333. [PubMed: 17406593]
28. Nnetu KD, et al. Directed persistent motion maintains sheet integrity during multicellular spreading and migration. Soft Matter. 2012; 8:6913.
29. Serra-Picamal X, et al. Mechanical waves during tissue expansion. Nat. Phys. 2012; 8:628–634.
30. Trepat X, et al. Physical forces during collective cell migration. Nat. Phys. 2009; 5:426–430.
31. Kim JH, et al. Propulsion and navigation within the advancing monolayer sheet. Nat. Mater. 2013; 12:856–863. [PubMed: 23793160]
32. Tambe DT, et al. Collective cell guidance by cooperative intercellular forces. Nat. Mater. 2011; 10:469–75. [PubMed: 21602808]
33. Angelini TE, et al. Glass-like dynamics of collective cell migration. Proc. Natl. Acad. Sci. 2011; 108:4714–4719. [PubMed: 21321233]
34. Park J-A, et al. Unjamming and cell shape in the asthmatic airway epithelium. Nat. Mater. 2015; 14:1040–1048. [PubMed: 26237129]
35. Garcia S, et al. Physics of active jamming during collective cellular motion in a monolayer. Proc. Natl. Acad. Sci. 2015; 112:15314–15319. [PubMed: 26627719]
36. Serra-Picamal X, et al. Mechanical waves during tissue expansion. Nat. Phys. 2012; 8:628–634.
37. Ng MR, Besser A, Danuser G, Brugge JS. Substrate stiffness regulates cadherin-dependent collective migration through myosin-II contractility. J. Cell Biol. 2012; 199:545–63. [PubMed: 23091067]
38. Matsubayashi Y, et al. 'White wave' analysis of epithelial scratch wound healing reveals how cells mobilise back from the leading edge in a myosin-II-dependent fashion. J. Cell Sci. 2011; 124:1017–21. [PubMed: 21402875]
39. Zehnder SM, Suaris M, Bellaire MM, Angelini TE. Biophysical Letter Cell Volume Fluctuations in MDCK Monolayers. Biophysj. 2015; 108:247–250.
40. Zaritsky A, et al. Propagating Waves of Directionality and Coordination Orchestrate Collective Cell Migration. PLoS Comput. Biol. 2014; 10:e1003747. [PubMed: 25058592]
41. Isa L, Besseling R, Morozov AN, Poon WCK. Velocity Oscillations in Microfluidic Flows of Concentrated Colloidal Suspensions. Phys. Rev. Lett. 2009; 102:58302.
42. Tlili S, et al. Waves in cell monolayer without proliferation: density determines cell velocity and wave celerity. 2016
43. Banerjee S, Utuje KJC, Marchetti MC. Propagating Stress Waves During Epithelial Expansion. Phys. Rev. Lett. 2015; 114:228101. [PubMed: 26196647]
44. Notbohm J, et al. Cellular Contraction and Polarization Drive Collective Cellular Motion. Biophys. J. 2016; 110:2729–2738. [PubMed: 27332131]
45. Vicsek T, Czirók A, Ben-Jacob E, Cohen I, Shochet O. Novel Type of Phase Transition in a System of Self-Driven Particles. Phys. Rev. Lett. 1995; 75:1226–1229. [PubMed: 10060237]
46. Hakim V, Silberzan P. Collective cell migration : a physics perspective. Reports Prog. Phys. 2017; doi: 10.1088/1361-6633/aa65ef
47. Solon AP, Chaté H, Tailleur J. From Phase to Microphase Separation in Flocking Models: The Essential Role of Nonequilibrium Fluctuations. Phys. Rev. Lett. 2015; 114:68101.
48. Chaté H, Ginelli F, Grégoire G, Raynaud F. Collective motion of selfpropelled particles interacting without cohesion. Phys. Rev. E. 2008; 77:46113.

49. Baskaran A, Marchetti MC. Enhanced Diffusion and Ordering of Self-Propelled Rods. Phys. Rev. Lett. 2008; 101:268101. [PubMed: 19113789]
50. Riveline D, et al. Focal Contacts as Mechanosensors. J. Cell Biol. 2001; 153
51. Trepat X, et al. Universal physical responses to stretch in the living cell. Nature. 2007; 447:592–595. [PubMed: 17538621]
52. Liu AJ, Nagel SR. Nonlinear dynamics: Jamming is not just cool any more. Nature. 1998; 396:21–22.
53. Trappe V, Prasad V, Cipelletti L, Segre PN, Weitz DA. Jamming phase diagram for attractive particles. Nature. 2001; 411:772–775. [PubMed: 11459050]
54. Briscoe J, Small S. Morphogen rules: design principles of gradient-mediated embryo patterning. Development. 2015; 142
55. Meinhardt H. Models for patterning primary embryonic body axes: The role of space and time. Semin. Cell Dev. Biol. 2015; 42:103–117. [PubMed: 26126935]
56. Oates AC, et al. Patterning embryos with oscillations: structure, function and dynamics of the vertebrate segmentation clock. Development. 2012; 139:625–39. [PubMed: 22274695]
57. Park J-A, Atia L, Mitchel JA, Fredberg JJ, Butler JP. Collective migration and cell jamming in asthma, cancer and development. J. Cell Sci. 2016; doi: 10.1242/jcs.187922
58. Ashby WJ, Wikswo JP, Zijlstra A. Magnetically attachable stencils and the non-destructive analysis of the contribution made by the underlying matrix to cell migration. Biomaterials. 2012; 33:8189–203. [PubMed: 22940214]
59. Solanas G, Cortina C, Sevillano M, Batlle E. Cleavage of E-cadherin by ADAM10 mediates epithelial cell sorting downstream of EphB signalling. Nat. Cell Biol. 2011; 13:1100–1107. [PubMed: 21804545]

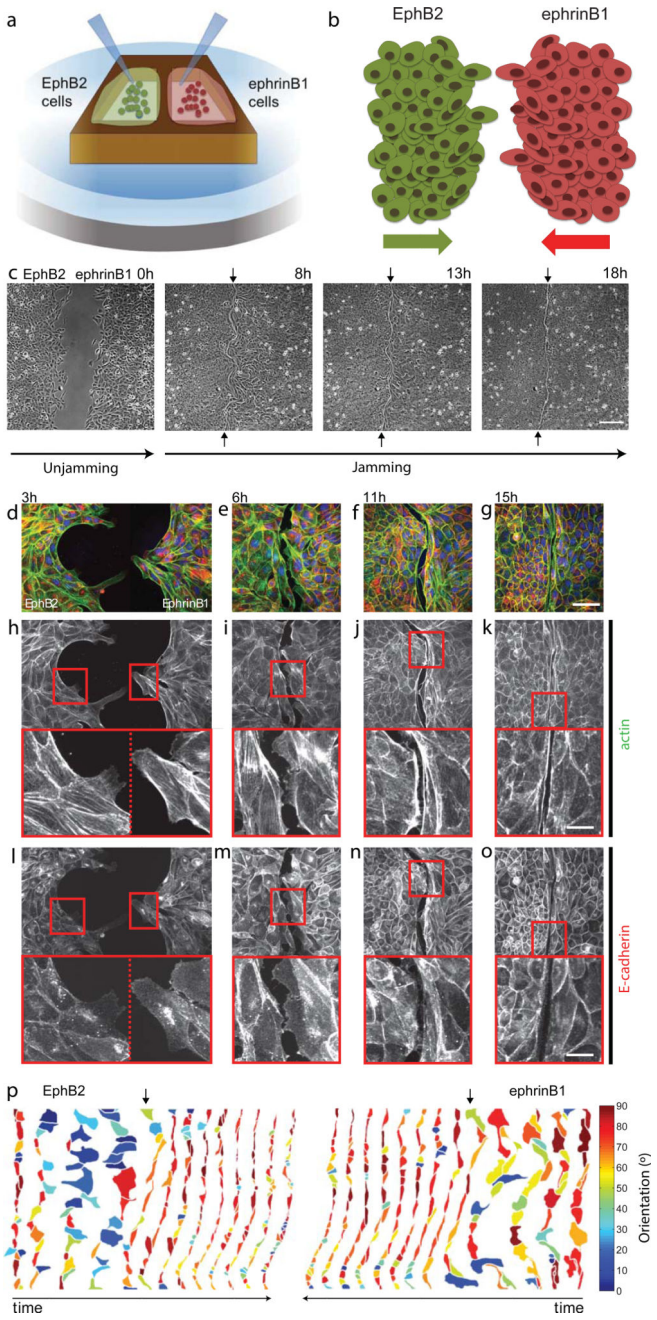

Figure 1. MDCK monolayers expressing EphB2 and ephrinB1 form a repulsive barrier

a-b, A magnetic PDMS stencil[58] with two cavities is attached to a collagen I-coated polyacrylamide (PA) gel using a magnet. Stable cell lines expressing EphB2 or ephrinB1 are seeded in each cavity of the stencil. After allowing cells to reach confluence the stencils are carefully removed and cells invade the surrounding space until both epithelia collide. **c**, Phase contrast images of EphB2/ephrinB1 boundary formation at different times after removal of the PDMS stencil (Scale bar is 220 μm). **d-g**, Merged staining of phalloidin (green), E-cadherin (red) and nuclei (blue) at different stages of boundary formation. Images are maximum projections of spinning disk z-stacks (Scale bar is 55 μm). **h-o**, Staining of

phalloidin (h-k) and E-cadherin (l-o) during boundary formation. Images are maximum projections of spinning disk z-stacks. Scale bar in zoomed regions is 18 μm. **p**, Time evolution of the first row of cells in the EphB2 (left) or ephrinB1 (right) monolayers color-coded according to their orientation with respect to the *x* axis. Time between frames is 105 min. Vertical arrows show the first time point after epithelial contact.

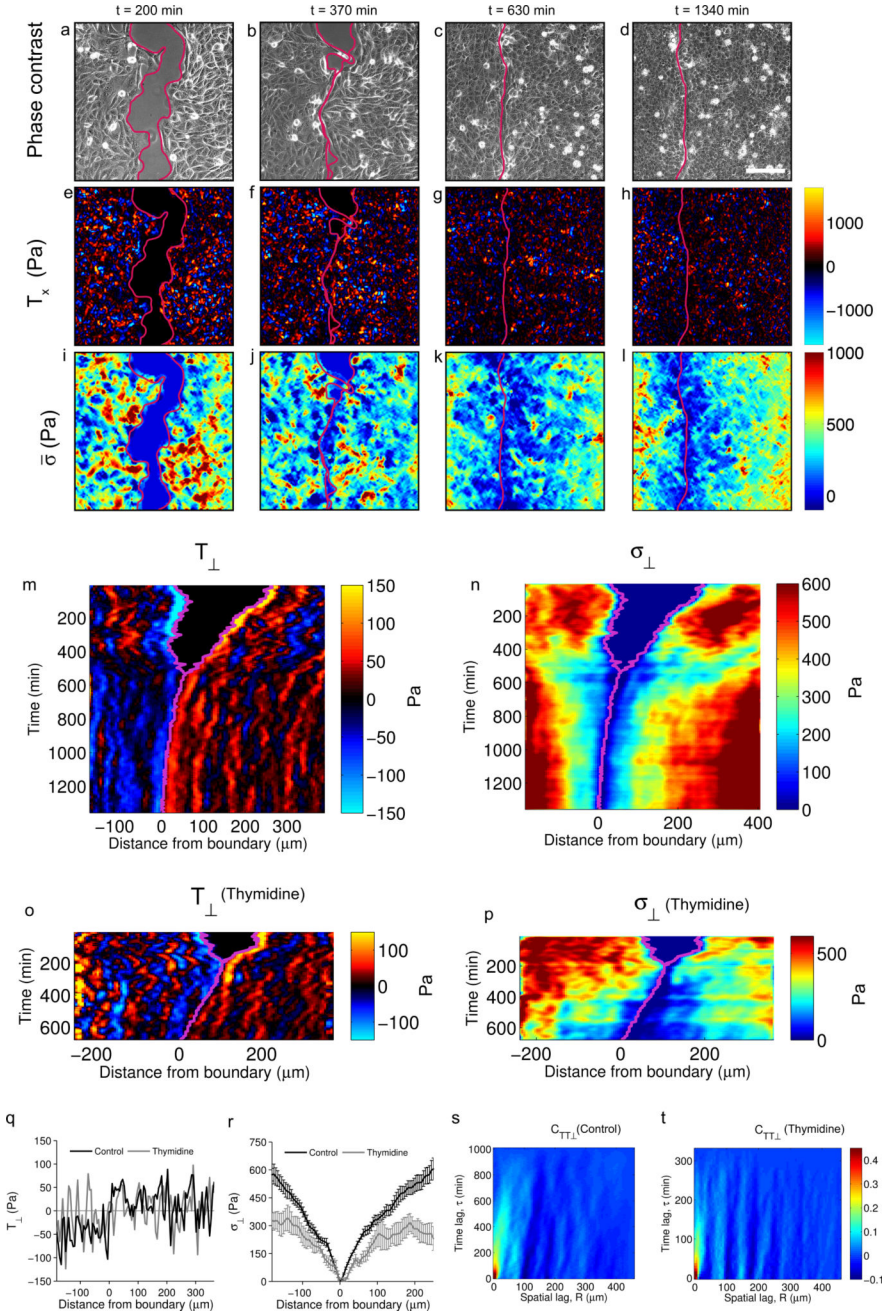

Figure 2. EphB2 and ephrinB1 monolayers exert supracellular oscillatory patterns of traction forces that pull cell-substrate adhesions away from the boundary

a–l, Phase-contrast images (a–d), horizontal traction component T_x (e–h) and average normal stress $\bar{\sigma}$ (i–l) at different times after removing the PDMS stencil. Scale bar, 150 μm. **m-p**, Kymographs of the traction $T_\perp$ (m,o) and monolayer stress component $\sigma_\perp$ (n,p) during the formation of an EphB2/ephrinB1 boundary in untreated cells (m,n) and cells treated with thymidine to inhibit proliferation (o,p). The purple line indicates the position of the boundary. **q-r**, Profile of $T_\perp$ (q) and $\sigma_\perp$ (r) at 420 minutes after epithelial contact for untreated monolayers and thymidine treated monolayers. **s-t**, Autocorrelation function $C_{TT\perp}$

of traction kymographs after contact for untreated cells (s) and thymidine treated cells (t). The appearance of periodic vertical bands in $C_{TT\perp}$ indicates oscillatory patterns that do not travel in time. Data are representative of n=6 independent experiments. See Supplementary Fig. 4 for additional repeats of kymographs.

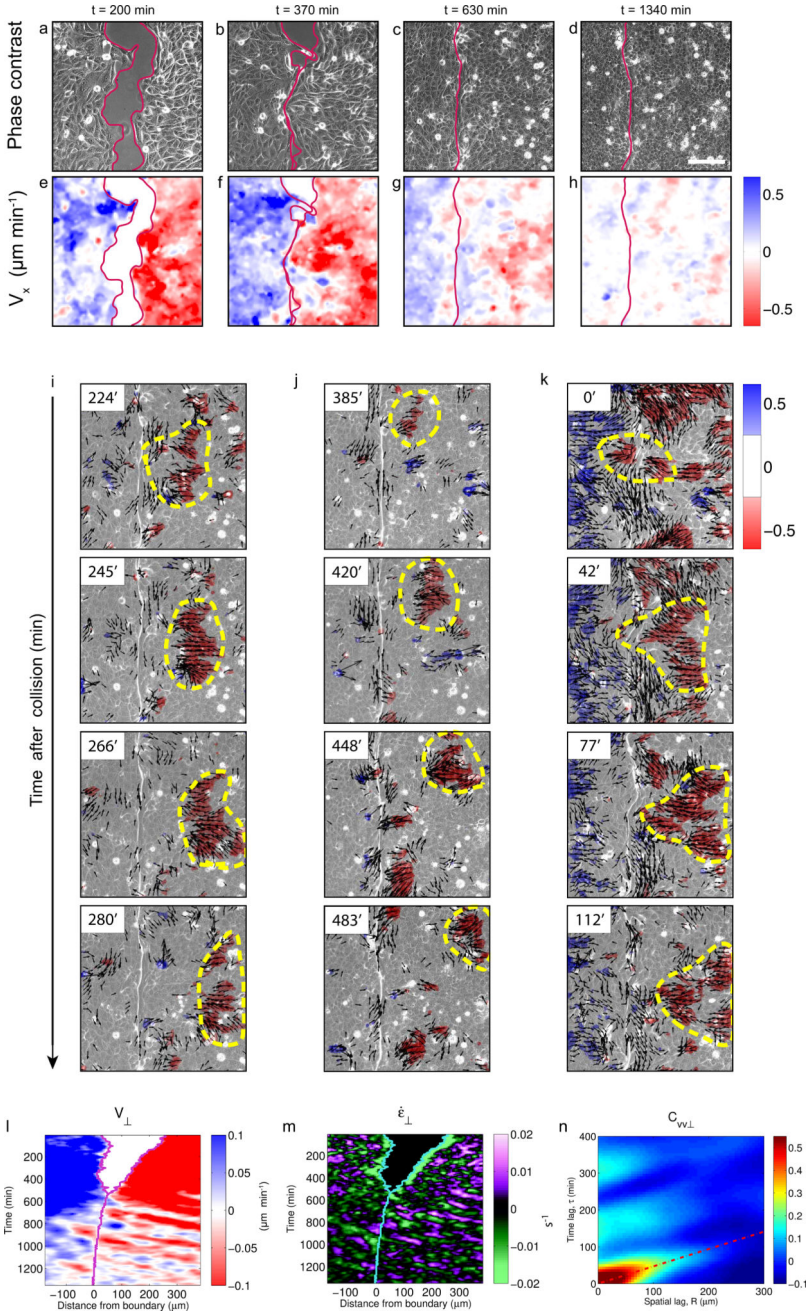

Figure 3. Deformation waves emerge at the monolayer boundary and propagate through the EphB2 monolayer

a-h, Phase-contrast images (a–d) and velocity V_X maps (e–h) at different time points after removing the PDMS stencil. Scale bar, 150 μm. **i-k**, Thresholded V_X fields superimposed on phase contrast images illustrate three examples of propagating fronts. Dashed yellow lines highlight clusters of high forward velocity propagating backwards at different time points (see supplementary Video 4 for a complete time-lapse recording). Arrows indicate the velocity vector (thresholded based on modulus). **l-m**, Kymographs of velocity $V_\perp$ (l) and strain rate $\dot{\varepsilon}_\perp$ (m) during EphB2/ephrinB1 boundary formation. The oblique bands

alternating sign indicate propagation of compression/extension pulses. **n**, Autocorrelation function $C_{VV\perp}$ of velocity kymographs for control cells during the jamming phase. The diagonal band in the autocorrelation function indicates propagation. The slope of the band is the inverse of the propagation velocity (117±16 μm/h). Average time between pulses is was 161±12 min. Data are representative of n=6 independent experiments. See Supplementary Fig. 4 for additional repeats of kymographs.

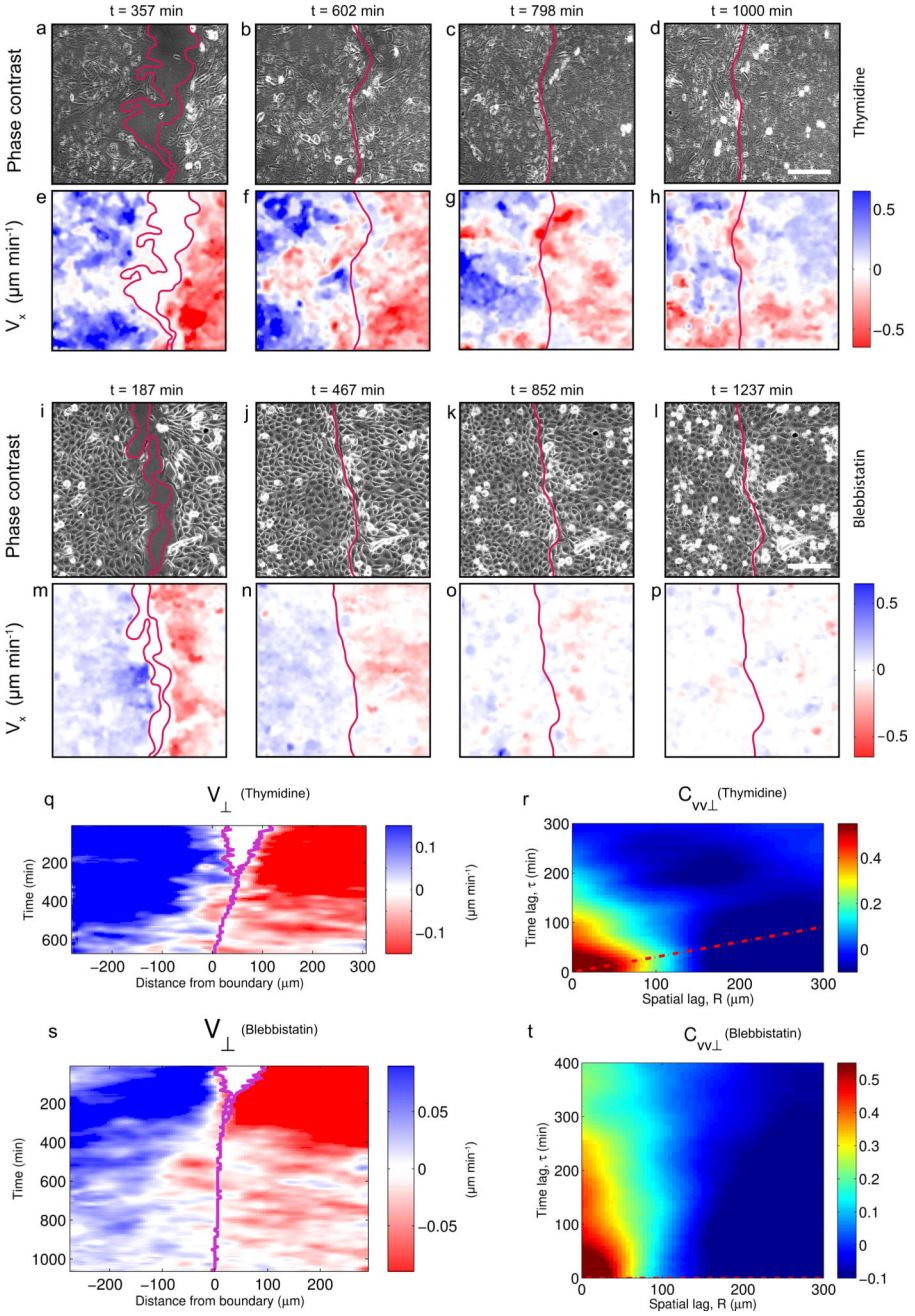

Figure 4. Deformation waves are attenuated by inhibition of proliferation and tension

a–h, Phase-contrast images (a–d) and velocity V_X (e–h) at different time points after removing the PDMS stencil in cells treated with thymidine to inhibit proliferation. Scale bar, 150 μm. **i–p**, Phase-contrast images (i–l) and velocity V_X (m–p) at different time points after removing the PDMS stencil in cells treated with blebbistatin to inhibit contractility. Scale bar, 150 μm. **q**, Kymograph of velocity $V_\perp$ for cells treated with thymidine. **r**, Autocorrelation function $C_{VV\perp}$ of velocity kymographs for cells treated with thymidine. **s**, Kymograph of velocity $V_\perp$ for cells treated with blebbistatin. **t**, Autocorrelation function

$C_{VV\perp}$ of velocity kymographs for cells treated with blebbistatin. Data are representative of n=3 independent experiments.

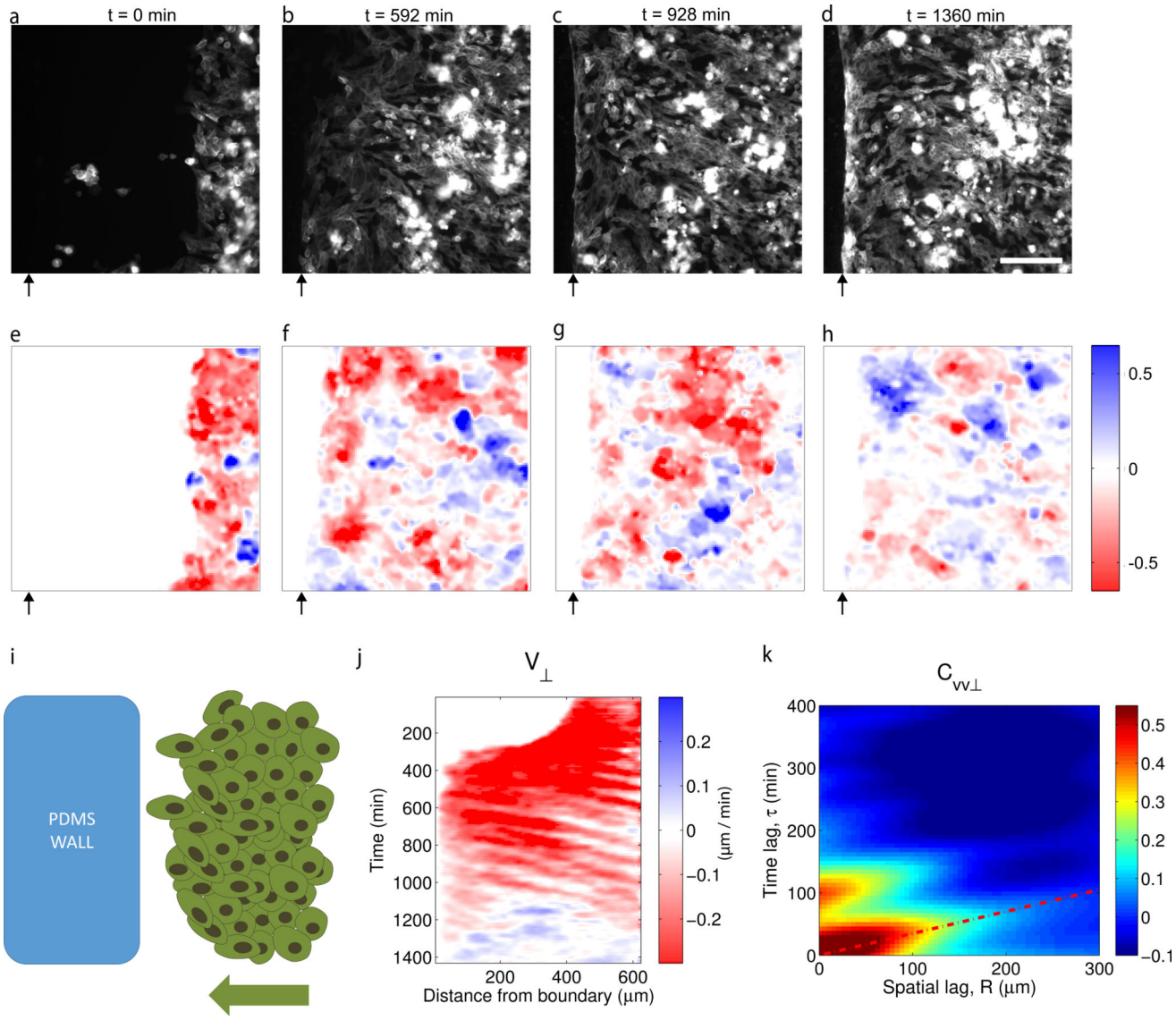

Figure 5. Deformation waves are a generic feature of repulsive interfaces during jamming

a–d, Fluorescence images of MDCK cells expressing EphB2 and lifeact-CFP during collision against a PDMS wall. **e-h**, Velocity component V_x corresponding to the time points indicated in a-d. Black arrows indicate the position of the wall. Scale bar, 150 μm. **i**, Scheme of the experimental design. **j**, Kymograph of velocity $V_\perp$. **k**, Autocorrelation function of $V_\perp$ after contact with the block. Average period between propagation events was 85±9 min. Average propagation velocity was 171±2 μm/h. Data are representative of n=3 independent experiments.

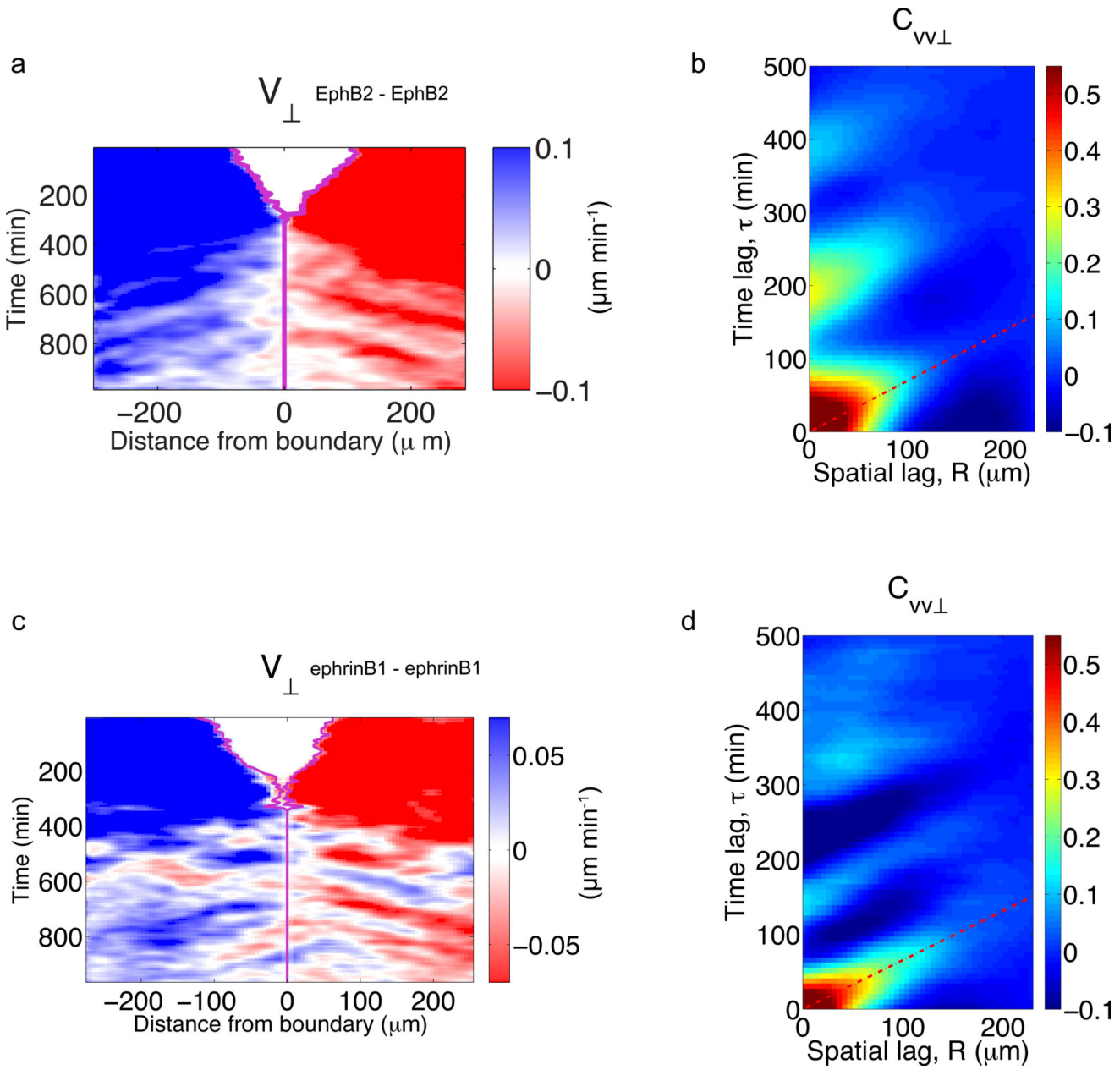

Figure 6. Deformation waves emerge during epithelial fusion

a, Kymograph of velocity $V_{\perp}$ during an EphB2/EphB2 homotypic collision. **b**, Autocorrelation function $C_{VV\perp}$ of velocity kymographs during the jamming phase of the EphB2/EphB2 collision. Average propagation velocity was 85±17 μm/h. **c**, Kymograph of velocity $V_{\perp}$ during an ephrinB1/ephrinB1 homotypic collision. **d**, Autocorrelation function $C_{VV\perp}$ of velocity kymographs during the jamming phase of the ephrinB2/ephrinB2 collision. Average propagation velocity was 112±20 μm/h. Data are representative of n=3 independent experiments per condition.